
# Metasurface constituted by thin composite beams to steer flexural waves in thin plates

Jun Zhang , Xiaoshi Su , Yaolu Liu , Youxuan Zhao , Yun Jing , Ning Hu

PII: S0020-7683(18)30478-5
DOI: https://doi.org/10.1016/j.ijsolstr.2018.11.025
Reference: SAS 10189

To appear in: *International Journal of Solids and Structures*

Received date: 26 May 2018
Revised date: 18 October 2018

Please cite this article as: Jun Zhang , Xiaoshi Su , Yaolu Liu , Youxuan Zhao , Yun Jing , Ning Hu , Metasurface constituted by thin composite beams to steer flexural waves in thin plates, *International Journal of Solids and Structures* (2018), doi: https://doi.org/10.1016/j.ijsolstr.2018.11.025

# Metasurface constituted by thin composite beams to steer flexural waves in thin plates

**Jun Zhang,[1,a)] Xiaoshi Su,[2] Yaolu Liu,[1] Youxuan Zhao,[1] Yun Jing,[3] and Ning Hu[1,b)]**

*[1] College of Aerospace Engineering, Chongqing University, Chongqing, 400044, P. R. China*
*[2]Mechanical and Aerospace Engineering, Rutgers University, Piscataway, New Jersey 08854, USA*
*[3] Department of Mechanical and Aerospace Engineering, North Carolina State University, Raleigh, North Carolina 27695, USA*

## ABSTRACT

We report a novel approach to control flexural waves in thin plates using metasurfaces constituted of an array of parallel arranged composite beams with their neutral planes the same as that of the host plate. The composite beams are composed of two connecting parts made of different materials, and have a thickness identical to that of the host plate. To steer flexural waves in thin plates, a rectangular zone is subtracted from the thin plate and is then filled with the designed metasurface. The time delay of flexural waves in each composite beam of the metasurface is tuned through the varying length of the two connecting components, while keeping the total length fixed. To quantitatively evaluate the time delay in each composite beam, a theoretical model for analyzing the phase of the transmitted flexural waves is developed based on both Mindlin plate theory and Timoshenko beam theory. To control the flexural waves at will, each composite beam in the metasurface is delicately designed according to the proposed theoretical model. For illustrative purposes, the refracted and focusing metasurfaces are designed and numerically validated.

## 1. Introduction

Thin plates are basic mechanical elements extensively employed in engineering (Evans and Porter, 2007) and consequently their dynamic behavior has been well explored (Climente et al., 2015; Evans et al., 2008; Norris and Vemula, 1995). Control of various elastic waves in them is of great benefit to the development of structural health monitoring, design of new micro-electro-mechanical system (MEMs) (Baboly

et al., 2018) , energy harvesting (Zareei et al., 2018), etc. To date, such control can be achieved in three popular forms of anomalous refraction (Farhat et al., 2010; Su et al., 2018; Su and Norris, 2016), focusing (Dubois et al., 2013; Tol et al., 2017; Torrent et al., 2014; Wu et al., 2011; Yan et al., 2013; Yi et al., 2016; Zareei et al., 2018), and cloaking (Brun et al., 2014; Cho et al., 2016; Colombi et al., 2015; Colquitt et al., 2014; Farhat et al., 2009a; Farhat et al., 2009b; Futhazar et al., 2015; Liu et al., 2016; Stenger et al., 2012; Zareei and Alam, 2017). As reported in the existing literature, there are two ways to control a wave: the active mode, through the employment of one or more physical fields (Chen et al., 2016; Yi et al., 2016), and the passive mode.

In this work, we pay attention only to the control of flexural waves in thin plates by refraction and focusing. Generally, such control can be realized through two approaches. One is the incorporation of additional sub-structures/elements deposited on the thin plates (Gusev and Wright, 2014), such as composite stubs constituted of silicone rubber and lead (Yan et al., 2013) and piezoelectric patches (Yi et al., 2016) attached to the thin plates, and through-holes (Wu et al., 2011) or blind holes (Tol et al., 2016, 2017) of different diameters drilled on the thin plates. It is well known that the speed of flexural waves in thin plates and beams is not only a function of material properties, but also highly depends on the thickness of plates and beams. Consequently, the other way to control flexural waves in thin plates is achieved through the spatial modulation of the thickness $h$ (Climente et al., 2013; Lefebvre et al., 2015; Zareei et al., 2018). Note that the critical physics behind both approaches is the same and is in tuning the local refractive index for flexural waves. For more details on the controlling of flexural and other waves in thin plates, we refer the reader to the review work of Zhu *et al*. (Zhu et al., 2015).

As mentioned above, the speed of flexural waves in thin plates and beams depends on both the material properties and the thickness $h$. In this work, instead of the thickness $h$ that has already been considered by others (Climente et al., 2013; Lefebvre et al., 2015; Su et al., 2018; Su and Norris, 2016; Zareei et al., 2018), the material properties are chosen to manipulate the flexural waves. The idea is that a

rectangular zone is subtracted from the thin plate to yield a hole, and the hole is then filled with a series of composite beams with the same thickness as the host plate. These composite beams are composed of two connecting parts made of different materials, one of which is the same as that of the host plate and the other is an otherwise isotropic and homogeneous material. The composite beams are parallel distributed with their axes along the propagation direction of the incident flexural wave and connected at two ends to the host plate. A small gap is reserved for adjacent beams to allow them to work as an individual beam. As the total length of the composite beam is fixed, the time delay of flexural waves through it can be tuned by different combinations of the two connecting parts. The metasurface, an aggregation of the composite beams, with a specific function to tune the flexural waves, can then be designed based on the proper selection of the composite beams.

The rest of this paper is organized as follows. The design of the metasurfaces and the transmission properties of the unit cell are introduced and analyzed in Sec. 2, with an emphasis on the phase modulation of the transmitted flexural waves by the varying length of the two connecting components of the composite beams. Two metasurfaces are designed and numerically verified using full finite-element-method (FEM) simulations to examine the proposed approach in Sec.3. Conclusions are presented in Sec. 4.

## 2. Design of metasurfaces and transmission properties

### *2.1 Description of metasurfaces*

Figure 1 shows the front and top views of a metasurface comprised of thin composite beams connected at two ends to a host plate with an identical thickness. The thickness, width, and length of the composite beams are denoted $h$, $b$, and $l$, respectively. The gap between two adjacent beams is denoted $a$, which is assumed to be much smaller than $b$. In this work, $h$=5 mm, $b$=3 mm, $l$=5 cm, and $a$=0.3 mm unless stated otherwise. All the composite beams are comprised of two kinds of materials, denoted materials 1 and 2, as shown in Fig. 1. Here, material 1 is selected

to be aluminum and material 2 is a material with a higher Young's-modulus-to-mass-density ratio. In fact, carbon-fiber-reinforced composite is an excellent candidate for material 2. In principal, other materials can also be used for material 2, provided that it has a higher Young's-modulus-to-mass-density ratio compared with material 1. The detailed properties for materials 1 and 2 used in this work are tabulated in Table 1. Variables $l_1$ and $l_2$ denote the lengths of the two connecting components of the composite beams. The ratio $l_1/l_2$ is defined as $\alpha$, which ranges from 0 to 1, representing distinct composite beams. As illustrated by the arrows in Fig. 1, the x direction indicates the propagation direction of flexural waves, while the z direction indicates the vibration of material particles.

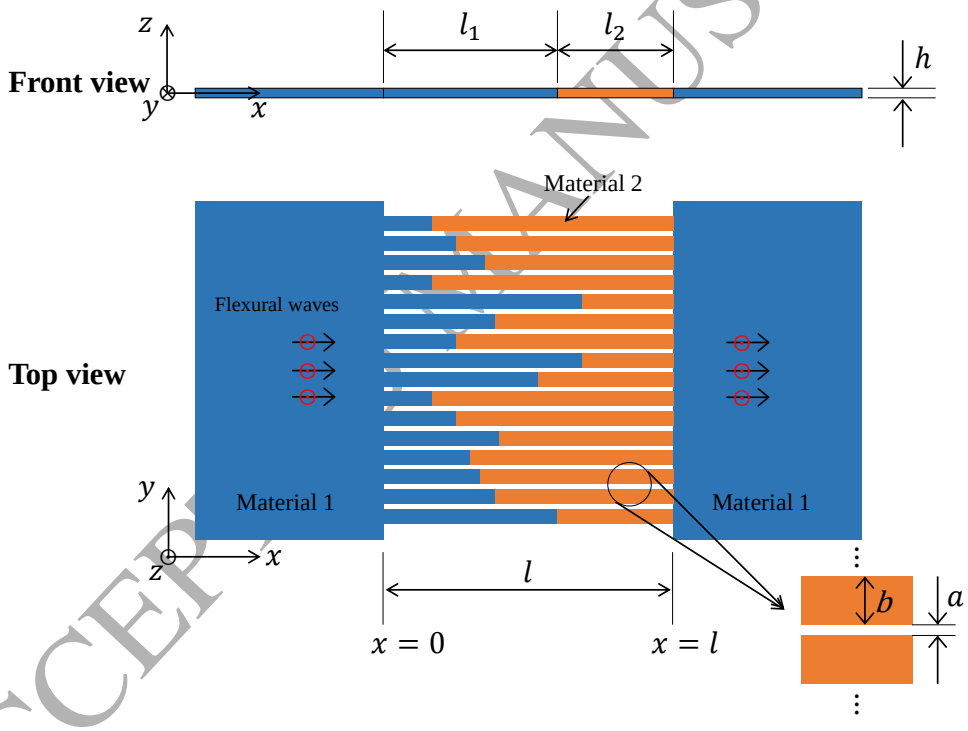


**Fig. 1.** Front and top views of metasurface made by parallel aligned thin composite beams to control flexural waves in thin plates. Different colors denote different materials.

Table 1. Materials used.

| Material | Young's modulus $E$ (Gpa) | Poisson's ratio $\upsilon$ | Mass density $\rho$ (kg/m$^3$) |
|---|---|---|---|
| 1 | 70.0 | 0.33 | 2700 |

| | | | |
|---|---|---|---|
| 2 | 500.0 | 0.31 | 2000 |

*2.2 Governing equations for flexural waves in thin plates and thin beams*

In this work, Young's modulus, shear modulus, Poisson's ratio, and mass density are denoted $E$, $\mu$, $\upsilon$, and $\rho$, respectively. Superscripts (1) and (2) indicate quantities associated with materials 1 and 2, respectively. Values for the plates and the beams are denoted by subscripts $p$ and $s$. Since the frequency of flexural waves considered in this work is relatively high, i.e. $kh > 1$, more accurate Mindlin plate and Timoshenko beam theory have been adopted to describe the dynamic behaviors of plates and beams.

In Mindlin plate theory (Su et al., 2018), the governing equation for flexural waves in a plate with a thickness $h$, in the absence of any external loading, is expressed as

$$\begin{aligned} &\mu\chi\left(\frac{\partial^2 w}{\partial x^2}-\frac{\partial \psi}{\partial x}\right)-\rho\frac{\partial^2 w}{\partial t^2}=0,\\ &D\frac{\partial^2 \psi}{\partial x^2}+\chi\mu\left(\frac{\partial w}{\partial x}-\psi\right)h-\lambda\frac{\rho h^3}{12}\frac{\partial^2 \psi}{\partial t^2}=0, \end{aligned} \tag{1}$$

where $w(x,t)$ is the out-of-plane displacement on the neutral plane and $\Psi(x,t)$ the bending angle. The bending stiffness of the plate is denoted $D = Eh^3/12(1-\upsilon^2)$, and $\chi$ and $\lambda$ are the shear and inertia correction factors, respectively, defined as

$$\begin{cases} \chi=\dfrac{20}{17-7\nu}\left(1+\sqrt{1-\dfrac{200(1-\nu)}{\chi_0(17-7\nu)^2}}\right)^{-1}, \\ \lambda=\chi/\chi_0, \end{cases} \tag{2}$$

based on the recent work of Norris (Norris, 2018), where $\chi_0 = \pi^2/12$. General solutions to Eq. (1) can be expressed in the form of travelling waves as $w(x,t) = \tilde{W}e^{\mathbf{i}(kx-\omega t)}$ and $\Psi(x,t) = \tilde{\Psi}e^{\mathbf{i}(kx-\omega t)}$, where $\mathbf{i}$ denotes an imaginary unit. Substituting the above two expressions for $w(x,t)$ and $\Psi(x,t)$ into Eq. (1) gives

$$\begin{pmatrix} \rho\omega^2-\mu\chi k^2 & -\mathbf{i}\mu\chi k \\ \mathbf{i}\mu\chi kh & \dfrac{\rho h^3}{12}\lambda\omega^2-Dk^2-\chi\mu h \end{pmatrix}\begin{pmatrix}\tilde{W}\\ \tilde{\psi}\end{pmatrix}=\mathbf{0}. \tag{3}$$

The equation for the wave number $k$ is then obtained

$$k^4 - \left(\frac{k_T^2}{\chi} + \lambda k_L^2\right)k^2 + \frac{\lambda k_T^2 k_L^2}{\chi} - k_F^4 = 0, \tag{4}$$

with $k_L = \omega\sqrt{\rho(1-\nu^2)/E}$, $k_T = \omega\sqrt{\rho/\mu}$, and $k_F = (\rho h\omega^2/D)^{1/4}$ representing the wave numbers of the longitudinal and transverse waves in two-dimensional plane-strain problems and the flexural waves in plates, respectively. Then, four solutions for $k$ are

$$\begin{aligned} k_{1,2} &= \pm\left\{\frac{1}{2}\left(\frac{k_T^2}{\chi} + \lambda k_L^2\right) + \sqrt{\frac{1}{4}\left(\frac{k_T^2}{\chi} - \lambda k_L^2\right)^2 + k_F^4}\right\}^{1/2}, \\ k_{3,4} &= \pm\left\{\frac{1}{2}\left(\frac{k_T^2}{\chi} + \lambda k_L^2\right) - \sqrt{\frac{1}{4}\left(\frac{k_T^2}{\chi} - \lambda k_L^2\right)^2 + k_F^4}\right\}^{1/2}, \end{aligned} \tag{5}$$

where $k_{1,2}$ are real and represent travelling waves, but $k_{3,4}$ are imaginary and correspond to evanescent waves as our frequency of interest $\omega < \frac{1}{h}\sqrt{12\mu\chi/\lambda\rho}$.

The corresponding governing equation for flexural waves in the beam of a thickness $h$ is expressed as:

$$\begin{aligned} \mu A\chi\left(\frac{\partial^2 w}{\partial x^2} - \frac{\partial \psi}{\partial x}\right) - \rho A\frac{\partial^2 w}{\partial t^2} &= 0, \\ EI\frac{\partial^2 \psi}{\partial x^2} + \mu A\chi\left(\frac{\partial w}{\partial x} - \psi\right) - \rho\lambda I\frac{\partial^2 \psi}{\partial t^2} &= 0, \end{aligned} \tag{6}$$

where $I = bh^3/12$ is the area moment of inertia and $A=b*h$ the cross-section area. Similarly, substituting the same expressions for $w(x,t)$ and $\Psi(x,t)$ as those for the plates into Eq. (6) gives

$$\begin{pmatrix} \rho\omega^2 - \mu\chi k^2 & -\mathbf{i}\mu\chi k \\ \mathbf{i}\mu\chi kA & \rho\lambda I\omega^2 - EIk^2 - \chi\mu A \end{pmatrix}\begin{pmatrix} \tilde{W} \\ \tilde{\psi} \end{pmatrix} = \mathbf{0}. \tag{7}$$

The equation for $k$ in Eq. (7) is the same as that for plates presented in Eq. (4), while the expressions for $k_L$ and $k_F$ are replaced by $k_L = \omega\sqrt{\rho/E}$ and $k_F = (\rho A\omega^2/EI)^{1/4}$, respectively. Four solutions for $k$ are also available, two of which are real and correspond to travelling waves, while the other two are imaginary as $\omega <$

$\frac{1}{h}\sqrt{12\mu\chi/\lambda\rho}$ and correspond to evanescent waves.

*2.3 Transmission of flexural waves through composite beam in metasurfaces*

To obtain the transmission spectrum of flexural waves through the composite beams in the designed metasurfaces, a unit cell between the two dashed lines shown in Fig. 2 was reproduced in the y direction to generate a fictional periodic structure. The unit cell is constituted by four parts labelled 1-4 as shown in Fig. 2. Under the incidence of a plane flexural travelling wave in the x direction, parts 1 and 2 can be assumed to be plane-strain beams, while parts 3 and 4 are directly taken as beams. The dynamic behavior of parts 1 and 4 can be described by Eq. (1), and Eq. (6) for parts 2 and 3. Hence, with the omission of time harmonic terms, the wave fields in the unit cell can be expressed as

$$W(x)=\begin{cases} e^{\mathbf{i}k_{p1}^{(1)}x}+R_1^{(1)}e^{\mathbf{i}k_{p2}^{(1)}x}+R_2^{(1)}e^{\mathbf{i}k_{p4}^{(1)}x}, & x<0,\\ A^{(1)}e^{\mathbf{i}k_{s1}^{(1)}x}+B^{(1)}e^{\mathbf{i}k_{s2}^{(1)}x}+U^{(1)}e^{\mathbf{i}k_{s3}^{(1)}x}+V^{(1)}e^{\mathbf{i}k_{s4}^{(1)}x}, & 0<x<l_1,\\ A^{(2)}e^{\mathbf{i}k_{s1}^{(2)}x}+B^{(2)}e^{\mathbf{i}k_{s2}^{(2)}x}+U^{(2)}e^{\mathbf{i}k_{s3}^{(2)}x}+V^{(2)}e^{\mathbf{i}k_{s4}^{(2)}x}, & l_1<x<L,\\ T_1^{(1)}e^{\mathbf{i}k_{p1}^{(1)}x}+T_2^{(1)}e^{\mathbf{i}k_{p3}^{(1)}x}, & x>L, \end{cases} \tag{8}$$

where $k_{\beta j}^{(i)}$ denote the wave numbers of four flexural waves ($j$=1, 2, 3, and 4) in the plate ($\beta$=$p$) or the beam ($\beta$=$s$) made of material $i$ ($i$=1,2). Parameters $R_i^{(1)}$, $A^{(i)}$, $B^{(i)}$, $U^{(i)}$, $V^{(i)}$, and $T_i^{(1)}$ ($i$=1, 2) are the 12 unknown coefficients that are determined by the continuity of out-of-plane displacements, bending angles, shear forces, and bending moments at the three interfaces of $x=0, l_1$ and $l$. The bending angles in both plates and beams are related to the out-of-plane displacements through Eq. (3) in the form

$$\psi(x)=\frac{\rho\omega^2-\mu\chi k^2}{\mathbf{i}\mu\chi k}W(x). \tag{9}$$

The shear force in the beam is $Q=\mu\chi hb\left(\frac{\partial W}{\partial x}-\Psi\right)$ and $Q=\mu\chi hb'\left(\frac{\partial W}{\partial x}-\Psi\right)$ in the plate, where $b'=b+a$. The bending moment in the beam is $M=EI\frac{\partial\Psi}{\partial x}$ and $M=Db'\frac{\partial\Psi}{\partial x}$ in the plate. Therefore, the equations governing the 12 unknowns can be

established. The detailed expressions for the linear system are given in the Appendix 1. Solving this system yields the unknowns.

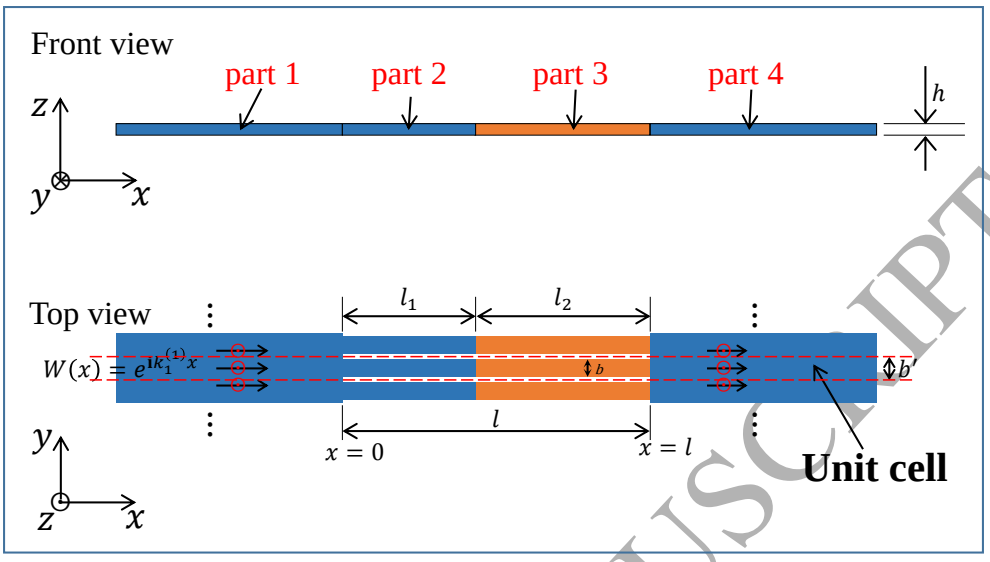


**Fig. 2.** Front and top views of unit cell used to analyze transmission spectrum of flexural waves through composite beams in designed metasurfaces. Incident wave is a plane flexural travelling wave. Black arrow denotes the propagation direction and red circle with dot the vibration direction of material particles.

Figure 3 shows the analytical magnitudes and phases of the transmitted waves at different frequencies. In this case, $\alpha$=0.5. It is evident that, the magnitude of the transmitted travelling wave ($T_1^{(1)}$) is considerably larger than that of the transmitted evanescent wave ($T_2^{(1)}$), which indicates that the transmitted evanescent wave is negligible.

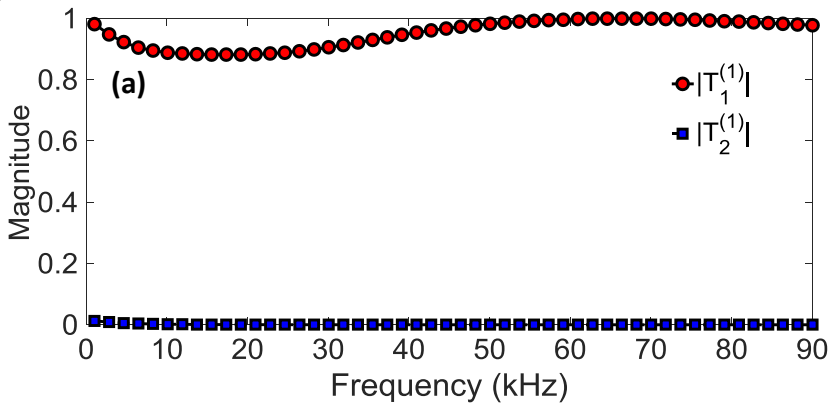

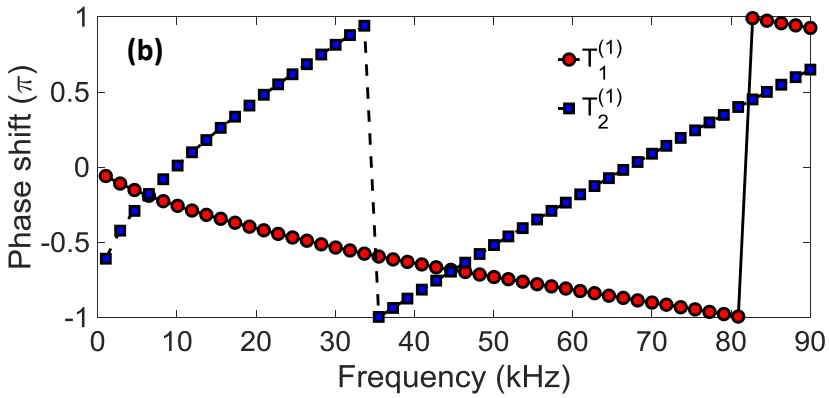


**Fig. 3.** Theoretical magnitudes (a) and phases (b) of transmitted waves changing with frequency.

The influence of $\alpha$ on the phase of the transmitted travelling wave ($T_1^{(1)}$) at four frequencies is illustrated in Fig. 4. The results indicate that changing of α is an effective way to make the phase of the transmitted travelling wave range from – π to π, particularly at higher frequencies. Therefore, according to the generalized Snell's law (Yu et al., 2011), it is possible that flexural waves in thin plates can be tuned by $\alpha$.

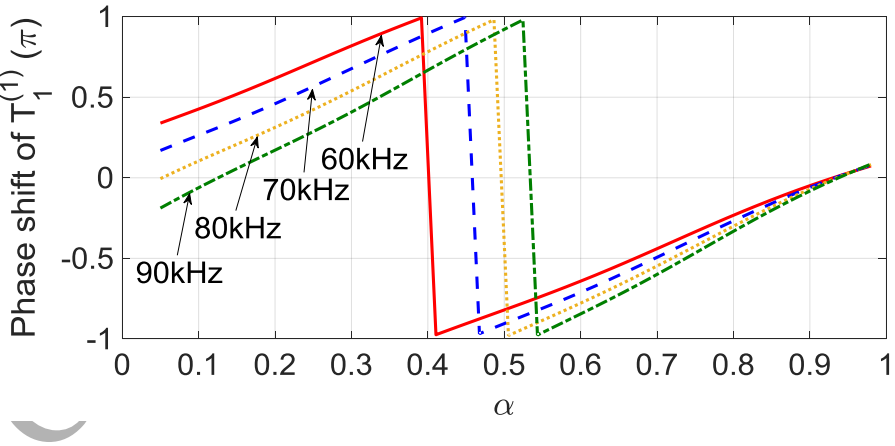


**Fig. 4.** Phases of transmitted travelling waves ($T_1^{(1)}$) changing with α at four different frequencies.

## 3. APPLICATIONS OF PROPOSED APPROACH

As an illustration for the applications of the idea proposed above, two numerical experiments were conducted. One is the design of a planar refraction lens and the other is a focusing lens, both for the flexural waves in thin plates.

*3.1 Planar refraction lens for flexural waves in thin plates*

A planar refraction lens for normal incident flexural waves propagating in thin plates was designed at 80 kHz. As an example, the angle of the refracted wave through this lens was set at 30°. According to the generalized Snell's law, for this case, 14 composite beams are selected from the phase of the transmitted travelling wave versus the α curve, as the solid dots show in Fig. 5. The detailed parameters for the 14 composite beams are tabulated in Table 2. It is worth mentioning that the transmitted travelling wave has a very high transmission coefficient, as illustrated in Table 2.

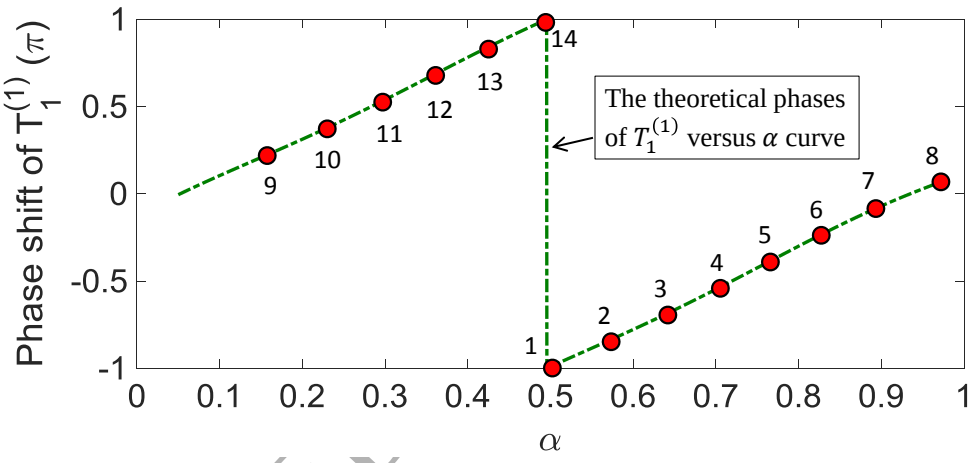


**Fig. 5.** Fourteen composite beams selected for planar refraction lens for flexural waves propagating in thin plates with refraction angle 30° at 80 kHz.

Table 2. Parameters of 14 composite beams constituting the lens with refraction angle 30° for flexural waves in thin plates at 80 kHz.

| No. | $\alpha$ | $\Phi(\pi)$ | $\lvert T_1^{(1)} \rvert$ |
|---|---|---|---|
| 1 | 0.5024 | -1.0000 | 0.9904 |
| 2 | 0.5735 | -0.8475 | 0.9973 |
| 3 | 0.6417 | -0.6950 | 0.9655 |
| 4 | 0.7052 | -0.5426 | 0.9307 |
| 5 | 0.7660 | -0.3901 | 0.9195 |
| 6 | 0.8271 | -0.2376 | 0.9329 |
| 7 | 0.8932 | -0.0851 | 0.9638 |
| 8 | 0.9722 | 0.0674 | 0.9968 |
| 9 | 0.1573 | 0.2199 | 0.9993 |
| 10 | 0.2299 | 0.3723 | 0.9710 |
| 11 | 0.2972 | 0.5248 | 0.9388 |

| | | | |
|---|---|---|---|
| 12 | 0.3610 | 0.6773 | 0.9339 |
| 13 | 0.4252 | 0.8298 | 0.9547 |
| 14 | 0.4941 | 0.9823 | 0.9872 |

To examine the performance of the designed lens, full numerical simulations in frequency domain using COMSOL® MultiPhysics software were conducted under its Solid Mechanics module. The numerical model is plotted in Fig. 6 with the inset showing the detailed structure of the designed lens, where the blue color represents material 1 and the gray material 2. In the numerical simulation, the entire domain was discretized using three-dimensional (3D) solid elements, and the perfectly matched layers (PMLs) were employed at the external zone to yield non-reflecting boundaries. To avoid rigid motion, the surfaces labelled 1, 2, and 3 and those on the other end were fixed in the x direction, and the surfaces labelled 4, 5 and the corresponding ones on the other side were not allowed to move in the y and z directions. A uniform out-of-plane displacement with a unit magnitude was applied on the dashed line AB to generate a plane flexural wave. Note that, such boundary conditions and applied loads were used in all the following simulations. The detail of geometries has been indicated in Fig. 6 (a). The simulated out-of-plane displacement fields shown in Fig. 6(d) indicate that the refracted wave is indeed at an angle of 30° with respect to the incident wave, which is in good agreement with the theoretically prescribed value. Although this lens was only designed for the single frequency of 80 kHz, numerical simulations at other frequencies, i.e., 75 and 90 kHz, were also conducted and the results illustrated in Fig. 7(a) and 7(b), respectively. The results show that the angle of the refracted wave is approximately 30° at 75 kHz and 26° at 90 kHz, which is slightly different from the predicted angle, i.e., 30°. It can be concluded that, although this lens was designed to work at a single frequency, it actually works reasonably well in a range of frequencies centered on the design frequency.

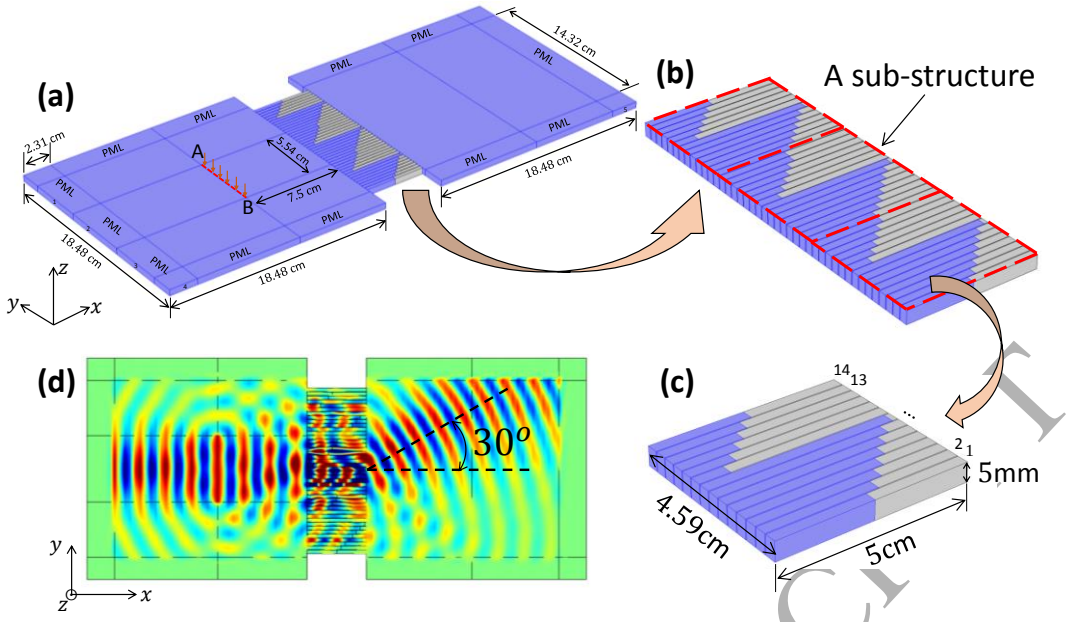


**Fig. 6.** Numerical simulation performed to examine feasibility of designed planar lens with refraction angle of 30° for flexural waves in thin plates at 80 kHz: (a) 3D view of numerical model, (b) lens constituted by three sub-structures, (c) detailed structure of sub-structure composed of 14 composite beams numbered 1-14, and (d) top view of out-of-plane displacements.

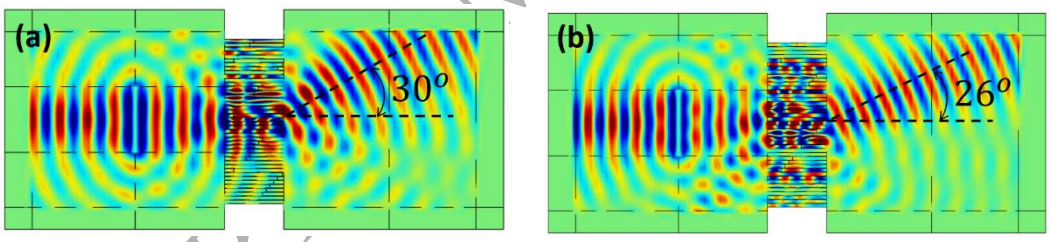


**Fig. 7.** Top view of simulated out-of-plane displacements for designed planar lens presented in Fig. 6 at (a) 75 and (b) 90 kHz.

As a further application, Fig. 8 shows the simulated out-of-plane displacement field for a designed wave-splitting lens. As shown in the inset, four sub-structures are employed in this lens, two of which are the same as that used in Fig. 6, while the detailed structure of the other two is illustrated in Fig. 8(c) and denoted sub-structure 2. They are constituted by 10 composite beams numbered 15-24 with detailed parameters listed in Table 3. They are properly selected according to the proposed theoretical model. The results indicate that the incident flexural wave is split into two parts and their propagation angles are found to be in good agreement with the

prescribed values of 30° and 45°. As before, numerical simulations were also conducted at other frequencies around the design frequency of 80 kHz, as illustrated by the results in Fig. 9. It is indicated in the figure that the refraction angle of the two split waves slightly changes from the prescribed 30° and 45°.

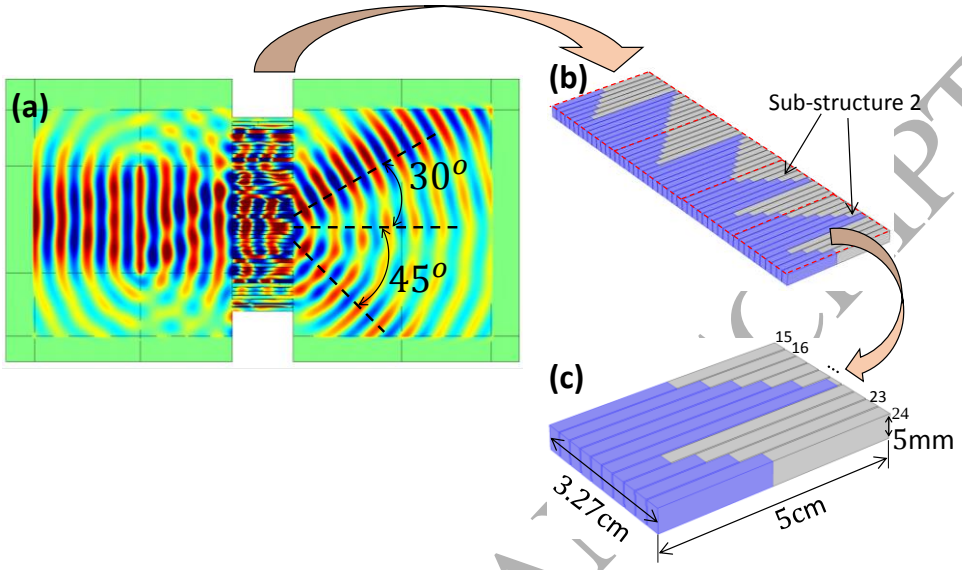


**Fig. 8.** Top view of simulated out-of-plane displacements (a) for designed splitter with refraction angles of 30° and 45° for flexural waves in thin plates at 80 kHz, (b) structure of the splitter, and (c) detailed structure of sub-structure 2.

Table 3. Parameters of 10 composite beams constituting sub-structure 2 used in the splitter for flexural waves in thin plates at 80 kHz.

| No. | $\alpha$ | $\Phi(\pi)$ | $\lvert T_1^{(1)} \rvert$ |
|---|---|---|---|
| 15 | 0.5024 | -1.0000 | 0.9904 |
| 16 | 0.6023 | -0.7844 | 0.9874 |
| 17 | 0.6944 | -0.5687 | 0.9354 |
| 18 | 0.7806 | -0.3531 | 0.9207 |
| 19 | 0.8696 | -0.1374 | 0.9517 |
| 20 | 0.9784 | 0.0782 | 0.9980 |
| 21 | 0.1933 | 0.2938 | 0.9894 |
| 22 | 0.2906 | 0.5095 | 0.9410 |
| 23 | 0.3809 | 0.7251 | 0.9381 |
| 24 | 0.4748 | 0.9408 | 0.9786 |

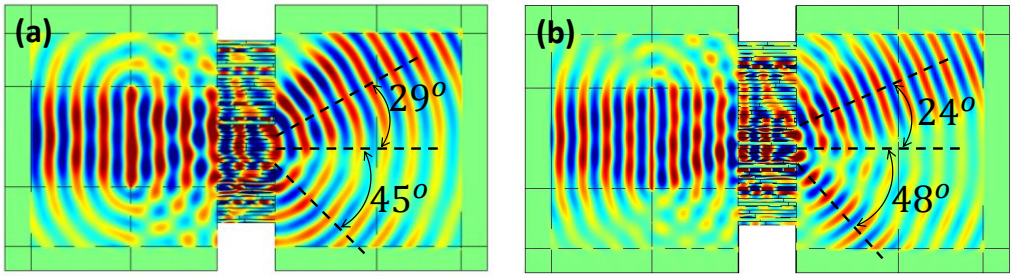


**Fig. 9.** Top view of simulated out-of-plane displacements for designed splitter presented in Fig. 8 at (a) 70 and (b) 90 kHz.

*3.2 Lens to focus flexural waves in thin plates*

A lens with a focal distance equals to 4 times the length of the composite beams was designed to focus flexural waves in thin plates. The required phase profile along the vertical direction is described by Eq. (19) in (Su et al., 2018). For this case, 54 composite beams are selected from the curve at 80 kHz presented in Fig. 4. Table A1 in the Appendix 2 lists the detailed parameters of these 54 beams, numbered from 1-54. As before, full numerical simulations were performed. The numerical model used and results are illustrated in Fig. 10 with the inset showing the designed metasurface. Results show that the wavefronts of the transmitted wave are concavely bent and the focal point is found to be approximately 17 cm from the metasurface, as illustrated in Fig. 10(e), which agrees with the designed focal distance to a remarkable degree.

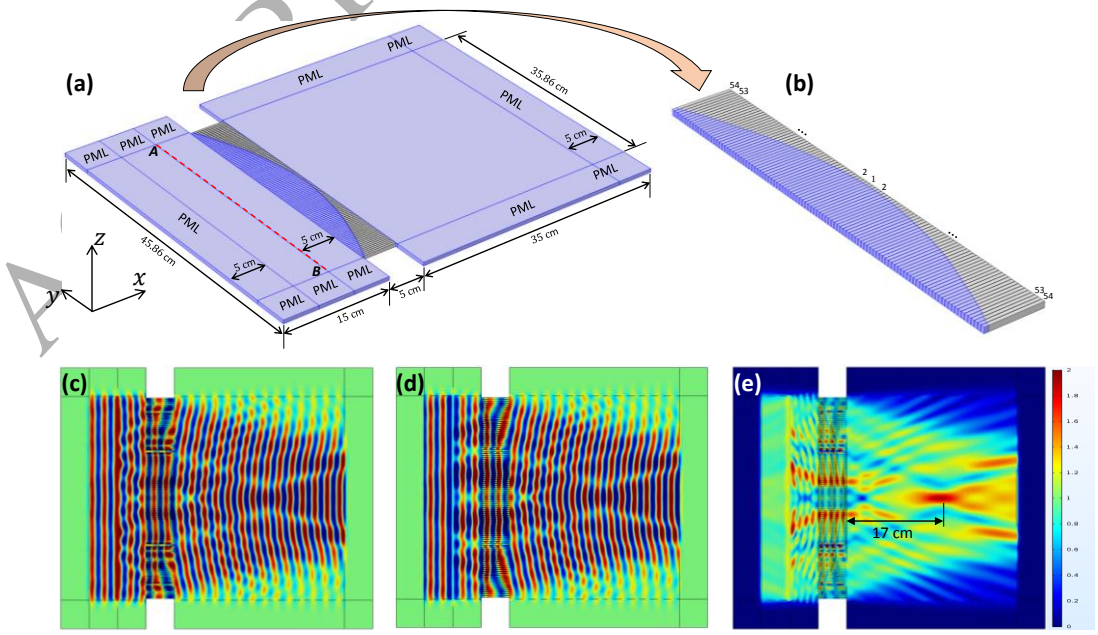

**Fig. 10.** Results of numerical simulation performed to examine feasibility of designed focusing lens with a focal distance of 20 cm for flexural waves in thin plates at 80 kHz: (a) 3D view of numerical model, (b) structure of designed metasurface, (c) top view of real part, (d) imaginary part, and (e) magnitude of out-of-plane displacements.

## 4. Conclusions

In conclusion, in this paper we proposed a novel approach for controlling flexural waves in thin plates using metasurfaces made of composite beams. The composite beams are made of two connecting parts with different materials. As the total length is fixed, different combinations of geometric size for the two parts yield distinct composite beams. A theoretical model based on Mindlin plate theory and Timoshenko beam theory was developed to evaluate transmission of flexural waves through such a composite beam connected at two ends to thin plates. Theoretical results indicate that phases of the transmitted travelling flexural wave can be tuned between $-\pi$ and $\pi$ by changing the lengths of the two connecting parts, indicating that the proposed composite beams are capable of steering flexural waves effectively. To examine the performance of the proposed idea, two numerical experiments were conducted. One was the design of a planar lens to refract flexural waves in thin plates and the other that of a focusing lens for flexural waves. The results of full numerical simulations verify the two designs. In addition to these two illustrative applications, this idea also benefits other applications, i.e., non-reciprocal propagation of flexural waves with the combination of phononic crystals.

## Acknowledgements

This work was supported by the Chinese National Natural Science Fund (Grants No. 11502036 and 11632004). The Key Program for International Science and Technology Cooperation Projects of the Ministry of Science and Technology of China (No. 2016YFE0125900), the Guangxi Key Laboratory of Manufacturing Systems and Advanced Manufacturing Technology (No:16-380-12-014k), and the Key Project of

Natural Science Foundation of CQ CSTC (No. cstc2017jcyjBX0063) also provided partial financial support.

**References**

Baboly, M.G., Reinke, C.M., Griffin, B.A., El-Kady, I., Leseman, Z.C., 2018. Acoustic waveguiding in a silicon carbide phononic crystals at microwave frequencies. Applied Physics Letters 112.

Brun, M., Colquitt, D.J., Jones, I.S., Movchan, A.B., Movchan, N.V., 2014. Transformation cloaking and radial approximations for flexural waves in elastic plates. New Journal of Physics 16.

Chen, Y., Hu, J., Huang, G., 2016. A design of active elastic metamaterials for control of flexural waves using the transformation method. Journal of Intelligent Material Systems and Structures 27, 1337-1347.

Cho, S., Yang, W., Lee, S., Park, J., 2016. Flexural wave cloaking via embedded cylinders with systematically varying thicknesses. Journal of the Acoustical Society of America 139, 3319-3323.

Climente, A., Norris, A.N., Sánchezdehesa, J., 2015. Scattering of flexural waves from a hole in a thin plate with an internal beam. Journal of the Acoustical Society of America 137, 293-302.

Climente, A., Torrent, D., Sanchez-Dehesa, J., 2013. Omnidirectional broadband insulating device for flexural waves in thin plates. Journal of Applied Physics 114.

Colombi, A., Roux, P., Guenneau, S., Rupin, M., 2015. Directional cloaking of flexural waves in a plate with a locally resonant metamaterial. Journal of the Acoustical Society of America 137, 1783-1789.

Colquitt, D.J., Brun, M., Gei, M., Movchan, A.B., Movchan, N.V., Jones, I.S., 2014. Transformation elastodynamics and cloaking for flexural waves. Journal of the Mechanics and Physics of Solids 72, 131-143.

Dubois, M., Farhat, M., Bossy, E., Enoch, S., Guenneau, S., Sebbah, P., 2013. Flat lens for pulse focusing of elastic waves in thin plates. Applied Physics Letters 103, 071915-071915-071914.

Evans, D.V, Porter, 2008. Flexural waves on a pinned semi-infinite thin elastic plate. Wave Motion 45, 745-757.

Evans, D.V., Porter, R., 2007. Penetration of flexural waves through a periodically constrained thin elastic plate in vacuo and floating on water. Journal of Engineering Mathematics 58, 317-337.

Farhat, M., Guenneau, S., Enoch, S., 2009a. Ultrabroadband Elastic Cloaking in Thin Plates. Physical Review Letters 103.

Farhat, M., Guenneau, S., Enoch, S., 2010. High directivity and confinement of flexural waves through ultra-refraction in thin perforated plates. Epl 91, 54003.

Farhat, M., Guenneau, S., Enoch, S., Movchan, A.B., 2009b. Cloaking bending waves propagating in thin elastic plates. Physical Review B 79.

Futhazar, G., Parnell, W.J., Norris, A.N., 2015. Active cloaking of flexural waves in

thin plates. Journal of Sound and Vibration 356, 1-19.
Gusev, V.E., Wright, O.B., 2014. Double-negative flexural acoustic metamaterial. New Journal of Physics 16.
Lefebvre, G., Dubois, M., Beauvais, R., Achaoui, Y., Ing, R.K., Guenneau, S., Sebbah, P., 2015. Experiments on Maxwell's fish-eye dynamics in elastic plates. Applied Physics Letters 106.
Liu, Y., Ma, Z., Su, X., 2016. Linear transformation method to control flexural waves in thin plates. Journal of the Acoustical Society of America 140, 1154-1161.
Norris, A., 2018. A refinement of Mindlin plate theory using simultaneous rotary inertia and shear correction factors. Journal of Vibration & Acoustics.
Norris, A.N., Vemula, C., 1995. Scattering of flexural waves on thin plates. Journal of Sound & Vibration 181, 115-125.
Stenger, N., Wilhelm, M., Wegener, M., 2012. Experiments on Elastic Cloaking in Thin Plates. Physical Review Letters 108.
Su, X., Lu, Z., Norris, A.N., 2018. Elastic metasurfaces for splitting SV- and P-waves in elastic solids. Journal of Applied Physics 123, 091701.
Su, X.S., Norris, A.N., 2016. Focusing, refraction, and asymmetric transmission of elastic waves in solid metamaterials with aligned parallel gaps. Journal of the Acoustical Society of America 139, 3386-3394.
Tol, S., Degertekin, F.L., Erturk, A., 2016. Gradient-index phononic crystal lens-based enhancement of elastic wave energy harvesting. Applied Physics Letters 109.
Tol, S., Degertekin, F.L., Erturk, A., 2017. Phononic crystal Luneburg lens for omnidirectional elastic wave focusing and energy harvesting. Applied Physics Letters 111.
Torrent, D., Pennec, Y., Djafari-Rouhani, B., 2014. Omnidirectional refractive devices for flexural waves based on graded phononic crystals. Journal of Applied Physics 116.
Wu, T.-T., Chen, Y.-T., Sun, J.-H., Lin, S.-C.S., Huang, T.J., 2011. Focusing of the lowest antisymmetric Lamb wave in a gradient-index phononic crystal plate. Applied Physics Letters 98.
Yan, X., Zhu, R., Huang, G., Yuan, F.-G., 2013. Focusing guided waves using surface bonded elastic metamaterials. Applied Physics Letters 103.
Yi, K., Collet, M., Ichchou, M., Li, L., 2016. Flexural waves focusing through shunted piezoelectric patches. Smart Materials and Structures 25.
Yu, N., Genevet, P., Kats, M.A., Aieta, F., Tetienne, J.-P., Capasso, F., Gaburro, Z., 2011. Light Propagation with Phase Discontinuities: Generalized Laws of Reflection and Refraction. Science 334, 333-337.
Zareei, A., Alam, M.R., 2017. Broadband cloaking of flexural waves. Physical Review E 95.
Zareei, A., Darabi, A., Leamy, M.J., Alam, M.R., 2018. Continuous profile flexural GRIN lens: Focusing and harvesting flexural waves. Applied Physics Letters 112.
Zhu, R., Liu, X.N., Hu, G.K., Yuan, F.G., Huang, G.L., 2015. Microstructural designs of plate-type elastic metamaterial and their potential applications: a review. International Journal of Smart and Nano Materials 6, 14-40.

**Appendix 1: Linear equations for 12 unknowns**

The continuity of out-of-plane displacements at locations $x = 0, l_1$ and $l$ yields,

$$\begin{cases} 1+R_1^{(1)}+R_2^{(1)} = A^{(1)}+B^{(1)}+U^{(1)}+V^{(1)}, \\ A^{(1)}z_{s1}^{(1)}+B^{(1)}z_{s2}^{(1)}+U^{(1)}z_{s3}^{(1)}+V^{(1)}z_{s4}^{(1)} = A^{(2)}z_{s1}^{(2)}+B^{(2)}z_{s2}^{(2)}+U^{(2)}z_{s3}^{(2)}+V^{(2)}z_{s4}^{(2)}, \\ A^{(2)}\hat{z}_{s1}^{(2)}+B^{(2)}\hat{z}_{s2}^{(2)}+U^{(2)}\hat{z}_{s3}^{(2)}+V^{(2)}\hat{z}_{s4}^{(2)} = T_1^{(1)}\hat{z}_{p1}^{(1)}+T_2^{(1)}\hat{z}_{p3}^{(1)}, \end{cases}$$

(**A1**)

with $z_{\beta i}^{(j)} = e^{\mathbf{i}k_{\beta i}^{(j)}l_1}$ and $\hat{z}_{\beta i}^{(j)} = e^{\mathbf{i}k_{\beta i}^{(j)}l}$, for $i$=1, 2, 3, 4; $j$=1, 2 and $\beta = p, s$.

The corresponding continuity of bending angles gives rise to

$$\begin{cases} p_{p1}^{(1)}+p_{p2}^{(1)}R_1^{(1)}+p_{p4}^{(1)}R_2^{(1)} = p_{s1}^{(1)}A^{(1)}+p_{s2}^{(1)}B^{(1)}+p_{s3}^{(1)}U^{(1)}+p_{s4}^{(1)}V^{(1)}, \\ p_{s1}^{(1)}A^{(1)}z_{s1}^{(1)}+p_{s2}^{(1)}B^{(1)}z_{s2}^{(1)}+p_{s3}^{(1)}U^{(1)}z_{s3}^{(1)}+p_{s4}^{(1)}V^{(1)}z_{s4}^{(1)} = \\ p_{s1}^{(2)}A^{(2)}z_{s1}^{(2)}+p_{s2}^{(2)}B^{(2)}z_{s2}^{(2)}+p_{s3}^{(2)}U^{(2)}z_{s3}^{(2)}+p_{s4}^{(2)}V^{(2)}z_{s4}^{(2)}, \\ p_{s1}^{(2)}A^{(2)}\hat{z}_{s1}^{(2)}+p_{s2}^{(2)}B^{(2)}\hat{z}_{s2}^{(2)}+p_{s3}^{(2)}U^{(2)}\hat{z}_{s3}^{(2)}+p_{s4}^{(2)}V^{(2)}\hat{z}_{s4}^{(2)} = \\ p_{p1}^{(1)}T_1^{(1)}\hat{z}_{p1}^{(1)}+p_{p3}^{(1)}T_2^{(1)}\hat{z}_{p3}^{(1)}, \end{cases} \quad (\mathbf{A2})$$

with $p_{\beta i}^{(j)} = \frac{\rho^{(j)}\omega^2-\mu^{(j)}\chi\left(k_{\beta i}^{(j)}\right)^2}{\mathbf{i}\mu^{(j)}\chi k_{\beta i}^{(j)}}$, for $i$=1, 2, 3, 4; $j$=1, 2 and $\beta = p, s$.

The equations for the 12 unknowns based on the continuity of shear forces are expressed as

$$\begin{cases} \alpha_{p1}^{(1)}+\alpha_{p2}^{(1)}R_1^{(1)}+\alpha_{p4}^{(1)}R_2^{(1)} = \frac{b}{b'}\left(\alpha_{s1}^{(1)}A^{(1)}+\alpha_{s2}^{(1)}B^{(1)}+\alpha_{s3}^{(1)}U^{(1)}+\alpha_{s4}^{(1)}V^{(1)}\right), \\ \alpha_{s1}^{(1)}A^{(1)}z_{s1}^{(1)}+\alpha_{s2}^{(1)}B^{(1)}z_{s2}^{(1)}+\alpha_{s3}^{(1)}U^{(1)}z_{s3}^{(1)}+\alpha_{s4}^{(1)}V^{(1)}z_{s4}^{(1)} = \\ \frac{\mu^{(2)}\chi^{(2)}}{\mu^{(1)}\chi^{(1)}}\left(\alpha_{s1}^{(2)}A^{(2)}z_{s1}^{(2)}+\alpha_{s2}^{(2)}B^{(2)}z_{s2}^{(2)}+\alpha_{s3}^{(2)}U^{(2)}z_{s3}^{(2)}+\alpha_{s4}^{(2)}V^{(2)}z_{s4}^{(2)}\right), \\ \alpha_{s1}^{(2)}A^{(2)}\hat{z}_{s1}^{(2)}+\alpha_{s2}^{(2)}B^{(2)}\hat{z}_{s2}^{(2)}+\alpha_{s3}^{(2)}U^{(2)}\hat{z}_{s3}^{(2)}+\alpha_{s4}^{(2)}V^{(2)}\hat{z}_{s4}^{(2)} = \\ \frac{\mu^{(1)}\chi^{(1)}b'}{\mu^{(2)}\chi^{(2)}b}\left(\alpha_{p1}^{(1)}T_1^{(1)}\hat{z}_{p1}^{(1)}+\alpha_{p3}^{(1)}T_2^{(1)}\hat{z}_{p3}^{(1)}\right), \end{cases} \quad (\mathbf{A3})$$

with $\alpha_{\beta i}^{(j)} = \mathbf{i}k_{\beta i}^{(j)} - p_{\beta i}^{(j)}$ for $i$=1, 2, 3, 4 and $j$=1, 2; $j$=1, 2 and $\beta = p, s$.

The continuity of the bending moment gives

$$\begin{cases} \tau_{p1}^{(1)} + \tau_{p2}^{(1)} R_1^{(1)} + \tau_{p4}^{(1)} R_2^{(1)} = \\ \dfrac{\left(1 - \nu^{(1)} * \nu^{(1)}\right) b}{b'} \left( \tau_{s1}^{(1)} A^{(1)} + \tau_{s2}^{(1)} B^{(1)} + \tau_{s3}^{(1)} U^{(1)} + \tau_{s4}^{(1)} V^{(1)} \right), \\ \tau_{s1}^{(1)} A^{(1)} z_{s1}^{(1)} + \tau_{s2}^{(1)} B^{(1)} z_{s2}^{(1)} + \tau_{s3}^{(1)} U^{(1)} z_{s3}^{(1)} + \tau_{s4}^{(1)} V^{(1)} z_{s4}^{(1)} = \\ \dfrac{E^{(2)}}{E^{(1)}} \left( \tau_{s1}^{(2)} A^{(2)} z_{s1}^{(2)} + \tau_{s2}^{(2)} B^{(2)} z_{s2}^{(2)} + \tau_{s3}^{(2)} U^{(2)} z_{s3}^{(2)} + \tau_{s4}^{(2)} V^{(2)} z_{s4}^{(2)} \right), \\ \tau_{s1}^{(2)} A^{(2)} \hat{z}_{s1}^{(2)} + \tau_{s2}^{(2)} B^{(2)} \hat{z}_{s2}^{(2)} + \tau_{s3}^{(2)} U^{(2)} \hat{z}_{s3}^{(2)} + \tau_{s4}^{(2)} V^{(2)} \hat{z}_{s4}^{(2)} = \\ \dfrac{E^{(1)} b'}{E^{(2)} b \left(1 - \nu^{(1)} * \nu^{(1)}\right)} \left( \tau_{p1}^{(1)} T_1^{(1)} \hat{z}_{p1}^{(1)} + \tau_{p3}^{(1)} T_2^{(1)} \hat{z}_{p3}^{(1)} \right), \end{cases} \quad \textbf{(A4)}$$

with $\tau_{\beta i}^{(j)} = \mathbf{i} k_{\beta i}^{(j)} * p_{\beta i}^{(j)}$ for $i$=1, 2, 3, 4 and $j$=1, 2; $j$=1, 2 and $\beta = p, s$.

## Appendix 2: Parameters for 54 composite beams

Table A1. Parameters of 54 composite beams constituting lens to focus flexural waves at 80 kHz.

| No. | $\alpha$ | $\Phi(\pi)$ | $\left\|T_1^{(1)}\right\|$ |
|---|---|---|---|
| 1 | 0.9352 | 0 | 0.9844 |
| 2 | 0.9346 | -0.0008 | 0.9842 |
| 3 | 0.9335 | -0.0032 | 0.9837 |
| 4 | 0.9313 | -0.0073 | 0.9828 |
| 5 | 0.9284 | -0.0129 | 0.9814 |
| 6 | 0.9247 | -0.0201 | 0.9797 |
| 7 | 0.9202 | -0.0290 | 0.9775 |
| 8 | 0.9149 | -0.0394 | 0.9750 |
| 9 | 0.9090 | -0.0515 | 0.9721 |
| 10 | 0.9023 | -0.0651 | 0.9686 |
| 11 | 0.8951 | -0.0802 | 0.9649 |
| 12 | 0.8872 | -0.0969 | 0.9609 |
| 13 | 0.8788 | -0.1152 | 0.9566 |
| 14 | 0.8699 | -0.1349 | 0.9521 |
| 15 | 0.8604 | -0.1562 | 0.9476 |
| 16 | 0.8505 | -0.1790 | 0.9429 |
| 17 | 0.8401 | -0.2033 | 0.9384 |
| 18 | 0.8293 | -0.2290 | 0.9340 |
| 19 | 0.8181 | -0.2561 | 0.9300 |
| 20 | 0.8063 | -0.2847 | 0.9264 |
| 21 | 0.7942 | -0.3147 | 0.9233 |
| 22 | 0.7815 | -0.3460 | 0.9210 |
| 23 | 0.7683 | -0.3788 | 0.9197 |
| 24 | 0.7547 | -0.4128 | 0.9195 |
| 25 | 0.7404 | -0.4482 | 0.9207 |

| | | | |
|---|---|---|---|
| 26 | 0.7256 | -0.4849 | 0.9235 |
| 27 | 0.7101 | -0.5229 | 0.9281 |
| 28 | 0.6939 | -0.5621 | 0.9346 |
| 29 | 0.6770 | -0.6025 | 0.9431 |
| 30 | 0.6593 | -0.6442 | 0.9531 |
| 31 | 0.6407 | -0.6870 | 0.9643 |
| 32 | 0.6212 | -0.7310 | 0.9758 |
| 33 | 0.6008 | -0.7762 | 0.9865 |
| 34 | 0.5794 | -0.8224 | 0.9948 |
| 35 | 0.5571 | -0.8698 | 0.9993 |
| 36 | 0.5341 | -0.9182 | 0.9993 |
| 37 | 0.5107 | -0.9677 | 0.9946 |
| 38 | 0.4872 | -1.0182 | 0.9861 |
| 39 | 0.4638 | -1.0697 | 0.9753 |
| 40 | 0.4406 | -1.1222 | 0.9637 |
| 41 | 0.4178 | -1.1756 | 0.9528 |
| 42 | 0.3950 | -1.2300 | 0.9436 |
| 43 | 0.3722 | -1.2853 | 0.9367 |
| 44 | 0.3493 | -1.3415 | 0.9328 |
| 45 | 0.3258 | -1.3986 | 0.9327 |
| 46 | 0.3018 | -1.4566 | 0.9369 |
| 47 | 0.2769 | -1.5153 | 0.9456 |
| 48 | 0.2510 | -1.5749 | 0.9583 |
| 49 | 0.2240 | -1.6353 | 0.9734 |
| 50 | 0.1958 | -1.6964 | 0.9884 |
| 51 | 0.1664 | -1.7584 | 0.9979 |
| 52 | 0.1360 | -1.8210 | 0.9996 |
| 53 | 0.1055 | -1.8844 | 0.9931 |
| 54 | 0.0754 | -1.9485 | 0.9809 |